Since January 2020 Elsevier has created a COVID-19 resource centre with free information in English and Mandarin on the novel coronavirus COVID-19. The COVID-19 resource centre is hosted on Elsevier Connect, the company's public news and information website.

Talanta 239 (2022) 123147

Contents lists available at ScienceDirect

Talanta

journal homepage: www.elsevier.com/locate/talanta

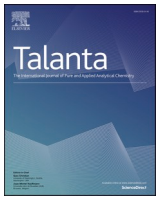

Rapid electrochemical immunodetection of SARS-CoV-2 using a pseudo-typed vesicular stomatitis virus model

Idan Ashur [a], Joel Alter [b], Michal Werbner [c], Abraham Ogungbile [a,d], Moshe Dessau [b], Meital Gal-Tanamy [c], Sefi Vernick [a,*]

[a] Department of Sensing, Information and Mechanization Engineering, Institute of Agricultural Engineering, ARO Volcani Center, 68 Hamaccabim Rd, Rishon lezion, 5025001, Israel
[b] The Laboratory of Structural Biology of Infectious Diseases, The Azrieli Faculty of Medicine, Bar-Ilan University, Safed, Israel
[c] Molecular Virology Lab, The Azrieli Faculty of Medicine, Bar-Ilan University, Safed, Israel
[d] Department of Soil and Water Sciences, Robert H. Smith Faculty of Agriculture, Food and Environment, The Hebrew University of Jerusalem, P.O. Box 12, Rehovot, 761001, Israel

ARTICLE INFO

Keywords:
Immunosensors
Electrochemical impedance spectroscopy
SARS-CoV-2 pseudovirus
COVID-19
Rapid diagnostic testing

ABSTRACT

The COVID-19 pandemic has highlighted the need for reliable and accurate diagnostic tools that provide quantitative results at the point of care. Real-time RT-PCR requires large laboratories, a skilled workforce, complex and costly equipment, and labor-intensive sample processing. Despite tremendous efforts, scaling up RT-PCR tests is seemingly unattainable. To date, hundreds of millions of COVID-19 tests have been performed globally, but the demand for timely, accurate testing continues to outstrip supply. Antigen-based rapid diagnostic testing is emerging as an alternative to RT-PCR. However, the performance of these tests, namely their sensitivity, is still inadequate. To overcome the limitations of currently employed diagnostic tests, new tools that are both sensitive and scalable are urgently needed. We have developed a miniaturized electrochemical biosensor based on the integration of specific monoclonal antibodies with a biochip and a measurement platform, and applied it in the detection of Spike S1 protein, the binding protein of SARS-CoV-2. Using electrochemical impedance spectroscopy, quantitative detection of sub-nanomolar concentrations of Spike S1 was demonstrated, exhibiting a broad detection range. To demonstrate the applicability of the biosensor, we have further developed a SARS-CoV-2 pseudovirus based on Spike protein-pseudo-typed VSV platform. Specific detection of different concentrations of pseudovirus particles was feasible in <30 min. This new tool may largely contribute to the fight against COVID-19 by enabling intensive testing to be performed and alleviating most of the hurdles that plague current diagnostics.

1. Introduction

While the aftermath of the COVID-19 pandemic is not yet on the horizon, the profound long-standing social, economic, and cultural effects are already beginning to unveil. Despite its devastating impact, however, the pandemic had accelerated research and development in many fields. In particular, new rapid diagnostic tests (RDT) have seen tremendous progress with noticeable applications already in use and many more in the pipeline, partly due to considerable government incentives.

Despite their obvious advantages, most Ag-RDT currently listed in FIND (Foundation for Innovative New Diagnostics) [1], demonstrate sensitivity and specificity of <80% and <97%, respectively. Consequently, in a setting with low prevalence of infection the positive predictive value (PPV) is significantly decreased, and the rate of false positives can be unacceptably high, rendering the test unusable or alternatively, requiring a confirmatory RT-PCR [2]. Thus, the variation of disease prevalence across populations and over time severely limits the widespread use of most Ag-RDT. Nevertheless, studies show that the often decreased sensitivity of antigen tests [3] might be offset if the point-of-care antigen tests are repeated frequently [4,5,6]. Currently, the sensitivity and specificity of Ag-RDT are insufficient and most

* Corresponding author. Department of Sensing, Information and Mechanization Engineering, Institute of Agricultural Engineering, ARO Volcani Center, P.O. Box 6, 68 Hamaccabim Rd, Rishon lezion, 5025001, Israel.
E-mail addresses: idana@volcani.agri.gov.il (I. Ashur), yoel.alter@biu.ac.il (J. Alter), michal.poran@gmail.com (M. Werbner), abraham.ogungbile@mail.huji.ac.il (A. Ogungbile), moshe.dessau@biu.ac.il (M. Dessau), Meital.Tanamy@biu.ac.il (M. Gal-Tanamy), sefi@volcani.agri.gov.il (S. Vernick).

https://doi.org/10.1016/j.talanta.2021.123147
Received 26 July 2021; Received in revised form 8 November 2021; Accepted 11 December 2021
Available online 13 December 2021

countries are still struggling with a diagnostic bottleneck.

Another impediment to the realization of new Ag-RDT is the requirement to conduct research in a professional biosafety level lab. In particular, validation of immunodiagnostic surface-based assays aimed at whole-virus particle detection involves viral culture growth that needs to be conducted in a BSL-3 laboratory [7]. A viable alternative is the use of pseudo-typed, non-replicative viral particles [8]. Pseudo-typed virus models usually involve incorporation of SARS-CoV-2 Spike protein onto other viruses such as retrovirus [9,10], lentivirus [11,12], MLV [13], and VSV [14,15,16]. The well-established VSV pseudovirus platform employs a VSV-ΔG vector that lacks the G envelope protein, thus facilitating recombination with a foreign reporter gene. Since they involve replication-defective viruses, the VSV pseudovirus platforms can be safely handled in a routine BSL-2 or lower [17] facilities. In fact, VSV pseudoviruses have been instrumental in the study of SARS-CoV-2 [18], including in the discovery of neutralizing antibodies [19], study of viral entry [20] and as quality control material in new nucleic acid detection test [21].

The majority of Ag-RDTs are equipped with a colorimetric readout [22,23]. In comparison, electrochemical detection methods are inherently more sensitive since they rely on direct transduction of electrons. Electrochemical biosensors comprising an electronic transducer functionalized with a biorecognition element are ideal candidates for on-site diagnostic devices. Direct electronic transduction of specific molecular binding into electrons avoids the use of optics, allows low-form-factor devices and delivers high signal levels. Furthermore, electrochemical biosensing is indifferent to sample turbidity, thus obviating the need for extensive sample purification steps. Finally, such devices are amenable to miniaturization and can be manufactured using conventional microelectronic fabrication techniques. Of the available techniques, electrochemical impedance spectroscopy (EIS) [24] is considered a powerful, label-free method that is optimally suited for point-of-care testing (POCT) [25]. The use of EIS-based (impedimetric) biosensors has been studied in the past decade with several reports, including the detection of metabolic disorder biomarkers [26,27] and bacterial infections [28,29]. The specificity of biosensors is mainly dependent on the utilized probe biomolecule. Integration of target-specific monoclonal antibodies (mAbs) as biorecognition elements (probes) is particularly promising since it combines the intrinsically high binding affinity and selectivity of mAbs with the sensitivity of electrochemical transduction. EIS-based biosensors for viral infections [30] have been demonstrated for influenza [31], Hepatitis E [32], Zika [33], Dengue [34] and more [35]. Impedimetric immunosensor for the detection of SARS-CoV-2 have recently been pursued [36], albeit with limited sensitivities and longer detection times.

We have developed a sensitive, accurate, reliable and easy-to-use immunobiosensor that enables a rapid POC detection of SARS-CoV-2. The biosensor is based on a miniaturized electrochemical chip, biofunctionalized with commercially available mAbs targeted against the conserved receptor-binding domain (RBD) of the SARS-CoV-2 spike protein. The chip, embedded in a portable biosensing platform, was applied in a rapid (<30min) and quantitative detection of spike proteins, exhibiting a wide dynamic range and sub-nanomolar sensitivity. We further demonstrate the feasibility of detecting various concentrations of spike-presenting whole-virus particles using a pseudo-typed VSV model. Validation of the biosensor with SARS-CoV-2 pseudoviruses serves as a proof of concept for a new generation of quantitative electrochemical Ag-RDT devices.

2. Materials and methods

In addition to the experimental details descried below, further details regarding chip fabrication and characterization; the PTFE-fabricated measurement platform; experimental procedures related to the biofunctionalization, and explanation of the EIS method and the Randles circuit are provided in the supplementary materials.

2.1. Chemicals, antibodies, and other reagents

Organic solvents (acetone, isopropanol), reagents (HCl, H_2O_2 30%, 2-Iminothiolane), and salts (KOH, $K_3Fe(CN)_6$, NaCl, KCl, KH_2PO_4, K_2HPO_4, NaH_2PO_4, Na_2HPO_4) were purchased from Sigma-Aldrich and used as received. All solutions were prepared with ultrapure water obtained from a Milli-Q water purifying system (≥18.2 MΩ cm^{-1}, Millipore). The antibodies/antigens used in this study were purchased from *Genscript*: SARS-CoV-2 Spike S1 Antibody (HC2001), Human Chimeric, which is an unconjugated recombinant human monoclonal IgG, Cat. No. A02038 (S1Ab). The antigens were: SARS-CoV-2 Spike protein (RBD, His & Avi tag) from human cells, Cat. No. Z03483, and, tag-free SARS-CoV-2 Spike protein (S1) from human cells, Cat. No. Z03501.

2.2. Electrochemical biosensor fabrication

Electrochemical biochips were designed (using CAD tools) as electrochemical cells with a three-electrode configuration (working, counter and reference planar electrodes). The electrodes were microfabricated on a p-doped Si/SiO_2 substrate (with 285 nm thermally grown oxide) by a 'Lift off' process. Electrodes were photolithographically patterned and then metal (Ti/Au 10nm/90 nm) was deposited by sputtering. The process flow is shown in Supplementary Fig. S1A. The working electrode diameter was 0.6 mm. On-chip reference electrodes (Ag/AgCl) were electroplated using an in-house electroplating bath, as shown in Supplementary Fig. S1B. Finally, individual chips were diced and their surface topology characterized by scanning electron microscopy, as shown in Supplementary Figs. S2A.

The quality of the electroplated Ag/AgCl quasi reference electrode (RE), and of the whole cell were electrochemically characterized. The RE potential demonstrated a linear dependence on the log of the electrolyte (NaCl) concentration, as expected, following the Nernst equation (Supplementary Fig. S2B).

2.3. Biofunctionalization

Antibodies were thiolated and immobilized to the gold working electrodes. For a detailed protocol, see Supplementary material section S4-S5. Briefly, Anti-S1 mAb (S1Ab) was immobilized onto the working electrode of electrochemical chips via thiol-modification of primary amines (-NH_2) of the S1Ab to introduce sulfhydryl (-SH) groups, thus allowing covalent immobilization of the thiolated antibodies to the gold electrode. S1Ab was then thiolated by incubation with Traut's reagent (2-Iminothiolane, 2-IT) at a molar ratio of 1:15 for 1 h at room temperature. Purification of the thiolated antibody was performed by centrifugation followed by dilution of the filtrate in 0.1 M phosphate buffer (pH 5). Prior to immobilization, the biochips were thoroughly cleaned and activated by 20 min immersion in solution of 50 mM KOH and 25% H_2O_2 followed by rinsing with ample amounts of Milli-Q water. The thiolated S1Ab was drop-casted onto the gold working electrode and left to react 2 h at 4 °C.

2.4. Preparation of SARS-CoV-2-spike pseudoparticles

To generate SARS-CoV-2 pseudo typed VSV particles, HEK-293 T cells were grown to 70% confluence in DMEM supplemented in 10% fetal bovine serum (FBS), 1% L-glutamine, 1% penicillin streptavidin and 1% non-essential amino acid. Cells were transfected with pCMV3 plasmid encoding the SARS-CoV-2 spike protein with C-terminal, 19 residues truncation (pCMV3-SARS-CoV-2-SΔ19) using polyethylenimine (PEI). Twenty-four hours post-transfection, the cells were infected with G-complemented $VSV^{GFP}\Delta G$ (*G-$VSV^{GFP}\Delta G$) at a multiplicity of infection (MOI) of 3. Following 6 h incubation to allow internalization, cells were extensively washed 4 times with fresh medium to eliminate excess of *G-$VSV^{GFP}\Delta G$. After additional 30 h of incubation the culture's supernatant containing pseudotyped VSV (SΔ19-

VSV^{GFP}ΔG) were centrifuged (300×*g*, 5 min, 4 °C), and stored at −80 °C until use.

To evaluate the pseudovirus titer, HEK-293 cells stably expressing hACE2 were cultured in Dulbecco's modified Eagle's medium (Gibco) supplemented in 10% fetal bovine serum (FBS), 1% L-glutamine, 1% penicillin streptavidin and 1% non-essential amino acid. These cells were seeded into 100 μg/mL poly-D-lysine-coated 96-well plates (Greiner) at an initial density of 0.5 × 10^5 cells per well. The following day, concentrated pseudo-particles were added to the 96-well pre-seeded plates. After 48 h, the cell medium was replaced with fresh DMEM excluding phenol red. 24 h later, the 96-well plates were imaged by the IncuCyte ZOOM system (Essen BioScience). Cells were imaged with a x10 objective using the default IncuCyte software settings, which were used to calculate number of GFP-positive cells from four 488 nm-channel images in each well (data were collected in triplicate), representing the number of infectious units. The final titer was evaluated as 1.5 × 10^6 pseudovirus/mL.

2.5. Measurement platform

Fabrication of the custom-made measurement platform is described in Supplementary section S5.

2.6. Electrochemical measurements

The quantitative detection of purified spike S1 protein solutions, S1 RBD and VSV pseudovirus was demonstrated using EIS measurements, as previously described in Ref. [37]. Briefly, EIS responses, recorded by a Biologic SP-300 instrument (BioLogic, Seyssinet-Pariset, France), were measured before and after functionalization, and after interaction of functionalized electrodes with either S1, or S1 receptor binding domain (RBD). The electrodes were gently washed with 3–5 mL of PBS to remove loosely bound species prior to each measurement. Acquisition of Nyquist plots in a solution of 10 mM $K_3Fe(CN)_6$ dissolved in 50 mM PBS pH 7.4 that contained 0.1 M KCl was performed by applying a potential of 220 mV with an alternating voltage amplitude of 5 mV at a frequency range of 10 kHz to 10 Hz. The charge transfer resistance (R_{ct}) was calculated by fitting the obtained plots to a Randel's equivalent circuit model. Binding of S1 and RBD proteins to immobilized S1Ab was achieved by drop casting of 15 μl purified protein, at the concentrations of 100 μg/mL of S1 or 0.015, 1.55, 15.5, and 1550 μg/mL of RBD, both in PBS, onto the working electrode surface followed by incubation for 30 min at 4 °C.

Whole virus detection by EIS: Stock solutions of SΔ19-VSV^{GFP}ΔG (with spike protein) and control pseudovirus *G-VSV^{GFP}ΔG (without spike protein) were filtrated by centrifugation and brought to a final volume of 250 μl in PBS to achieve an estimated concentration of ~2 × 10^7 particles/mL for each sample. Both species were interacted with S1Ab-modified electrodes similarly to S1 and RBD proteins. EIS responses were measured immediately after incubation (30 min at 4 °C), and after subsequent incubation in PBS for 15 min at room temperature under mild shaking. Dependence of R_{ct} on SΔ19-VSV^{GFP}ΔG concentration was carried out using SΔ19-VSV^{GFP}ΔG concentrations of 0.008, 0.08, 0.8, 8.0, and 800 × 10^7 particles/mL.

3. Results

Impedimetric biosensors show great promise in rapidly detecting low concentrations of target antigens within a highly simplified testing setup. We sought to demonstrate the immunodiagnostic potential by developing a miniature electrochemical biochip, integrating it with a monoclonal antibody (mAb) specific to the receptor-binding domain (RBD) of spike protein S1 subunit, and applying the developed immunosensor in the rapid detection of low concentrations of spike protein and spike-presenting whole virus particles. A schematic illustration of the developed biochip is presented in Fig. 1A.

Multiple electrochemical cells were fabricated and bio-functionalized to enable detection of purified spike proteins or spike-presenting pseudoviruses. Nyquist plots, generated by Electrochemical Impedance Spectroscopy (EIS) measurements, were fitted to an equivalent electric circuit from which charge transfer resistance (R_{ct}) values were extracted, as shown in Fig. 1B (See Supplementary material section S3 for further description of the EIS method).

The developed biochip, comprising an electrochemical cell with a three-electrode configuration, was fabricated on a Si/SiO_2 substrate using conventional microelectronic fabrication technology. A robust process was optimized for wafer-scale manufacturing with a yield of

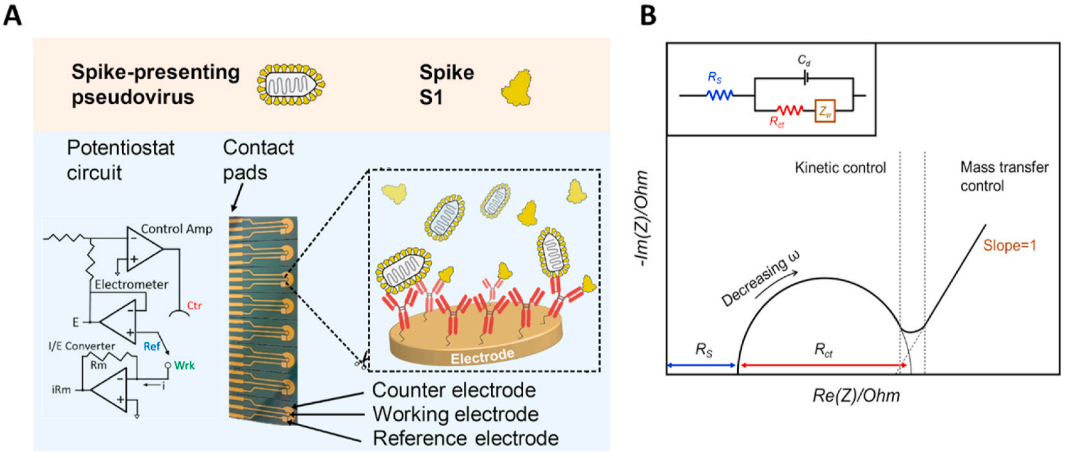

Fig. 1. EIS-based biosensor for SARS-CoV-2 detection. A) An illustration of the developed biochip and detection method. Multiple electrochemical cells are fabricated by microelectronic manufacturing techniques. Anti-spike S1 mAbs are chemically modified and covalently immobilized to an activated gold working electrode surface. The biochip is interfaced with a portable potentiostat device (a generalized circuit diagram is shown on the left). A brief incubation with samples containing soluble spike proteins or whole virions results in specific binding of the proteins/particles to the electrode-bound antibodies, affecting the electrode's impedance. This change can be measured and analyzed in real-time, allowing the quantification of spike proteins or particles in the sample. B) EIS is used to interrogate an electrochemical system and allows to separate the individual components that affect the resistance. The change in the "real" component of the impedance (Z′ or Z_{real}) versus the "imaginary" component (Z″ or -Z_{imag}, which results from capacitance), over a range of frequencies is known as a Nyquist plot. The generated Nyquist plot is fitted to an equivalent electric circuit from which the different resistance values are extracted (inset). Solution resistance, R_s, charge transfer resistance, R_{ct}, Warburg resistance, Z_w, and double layer capacitance, C_{dl}, can all be modeled and calculated. (For interpretation of the references to color in this figure legend, the reader is referred to the Web version of this article.)

~80%, as shown in Supplementary Fig. S1A. An on-chip Ag/AgCl quasi-reference electrode was also electroplated to enable miniaturization and consequently, high-throughput measurements (shown in Supplementary Fig. S1B). Biochips were thoroughly characterized prior to experiments, as shown in Supplementary Figs. S2 and S3. Finally, biochips were mounted onto a custom-designed, Polytetrafluoroethylene (PTFE) measurement platform, shown in Supplementary Fig. S4. The compact measurement platform provided electrical contacts to multiple biochips, thus allowing their simultaneous interrogation by a potentiostat device.

Impedimetric immunosensors are based on an antibody-functionalized electrode to detect antigens using EIS. The immobilization strategy of antibodies determines the coverage, orientation and ultimately, the observed signal response [38]. A direct immobilization approach is based on the covalent attachment of thiolated antibodies to a gold electrode surface. Activated gold surfaces can be readily reacted with the sulfur head of thiolated biomolecules enabling their immobilization [39]. Accordingly, sulfhydryl groups were introduced onto anti-spike S1 subunit mAb (S1Ab) and the resulted thiolated antibodies were immobilized onto activated electrodes. The reaction mechanism is detailed in Supplementary material section S4 and Fig. S5.

To measure the effect of immobilized antibodies on the R_{ct}, impedance spectra were recorded and analyzed before and after antibody immobilization, and these were compared with measurements taken after 30 min of incubation with S1 (or S1 receptor-binding domain (RBD)), as shown in Fig. 2A. Using the Nyquist plots, we observed the effect of antibody immobilization on the R_{ct}, represented by the gradually increasing semicircle diameters. In a bare electrode, the R_{ct} is small (283 Ω ± 9) and impedance is dominated by the diffusion of the electroactive species, the so-called Warburg impedance, which is evident in low frequencies [40]. Following antibody immobilization, the Warburg impedance is no longer a significant factor. Instead, the contribution of R_{ct} to the impedance becomes largely dominant, due to the addition of molecular layers on the electrode surface (R_{ct} = 781 Ω ± 235). A brief Incubation with a solution containing 100 μg/mL spike protein S1 subunit was found to significantly affect the impedimetric signal, resulting in a further increase in R_{ct} (2215 Ω ± 264), as the bound protein adds to the resistive component of the impedance. A bar graph of the corresponding R_{ct} values, calculated by fitting the Nyquist plots to Randel's equivalent circuit model, is shown in Fig. 2B (See Supplementary material section S3-S4 for a detailed description of the Randel's equivalent circuit model).

We further explored the sensitivity performance and dynamic range of the biosensor by examining its response to varying RBD concentrations, spanning five orders of magnitude. Fig. 2C shows the relative increase of R_{ct} (ΔR_{ct}, calculated by: $[R_{ct}(RBD)/R_{ct}(S1Ab)]$-1) following incubation with RBD. Specific signal was observed already at 15 ng/mL. The addition of RBD was found to affect R_{ct} in a dose-dependent manner, where the observed increase of ΔR_{ct} was exponentially dependent on RBD concentration, as seen in Fig. 2D. Supplementary Table 1 contains a detailed list of the obtained $\%\Delta R_{ct}$ values.

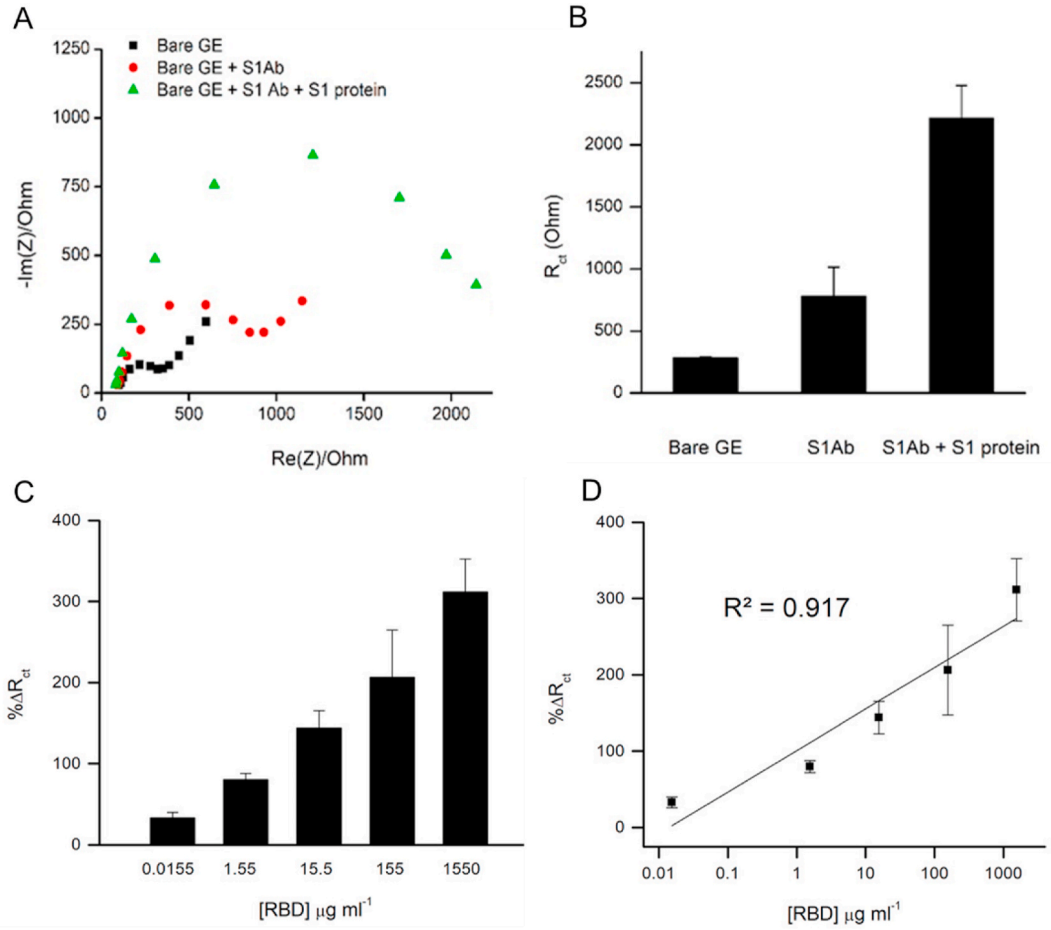

Fig. 2. The Concentration-dependent effect of Spike S1 binding on charge transfer resistance. A) Representative Nyquist plots from measurements of a bare gold electrode (denoted 'Bare GE', black squares), S1Ab-functionalized electrode ('Bare GE + S1Ab', red circles), and S1Ab-functionalized electrode after incubation in a solution containing 100 μg/mL purified S1 ('Bare GE + S1Ab + S1 protein', green triangles); B) the corresponding R_{ct} values averaged over 3–5 repetitions. C) Relative R_{ct} change obtained for different S1-RBD concentrations (0.015, 1.55, 15.5, 155 and 1550 μg/mL). ΔR_{ct} values were calculated by: $[R_{ct}(RBD)/R_{ct}(S1Ab)]$-1 and averaged over 3 to 5 repetitions; D) Dependence of $\%\Delta R_{ct}$ on RBD concentration. Error bars represent ±SD. (For interpretation of the references to color in this figure legend, the reader is referred to the Web version of this article.)

The applicability of new Ag-RDT devices is strongly dependent on their binding capacity to soluble Spike proteins and their context in the virus particle assembly. To this end, we have recently developed a Vesicular stomatitis virus (VSV)-based pseudoviruses that present SARS-CoV-2 Spike on their membrane as well as encoding a GFP reporter gene to monitor infectivity (SΔ19-VSV^{GFP}ΔG). These pseudo-typed particles were used to infect hACE2-expressing HEK-293 cells (HEK293^{hACE2}) at various MOI (multiplicity of infection). As a positive control, we generated pseudovirus expressing VSV-G protein (VSVΔG-G). The number of cells expressing the GFP reporter gene represents the number of infectious viruses and the pseudovirus' titer was determined by calculation of virus particles per 1 mL as shown in Fig. 3.

We examined the applicability of the biosensor in detecting spike protein-presenting pseudoviruses, by incubating samples containing an estimated 2×10^7/mL SΔ19-VSV^{GFP}ΔG pseudoparticles on the biochip and measuring the impedance response. As seen from the representative Nyquist plots of Fig. 4A, the impedance spectra were significantly affected following S1Ab functionalization and after incubation with SΔ19-VSV^{GFP}ΔG. Higher R_{ct} values were consistently recorded for SΔ19-VSV^{GFP}ΔG (mean $R_{ct} = 2.6{\cdot}10^3$ Ω ±315) compared to the S1Ab-functionalized electrode (mean $R_{ct} = 1.6{\cdot}10^3$ Ω ±82), as shown in Fig. 4B and in Supplementary Table 2. In order to exclude possible temporary increase of R_{ct} due to physically adsorbed virus entities rather than specific antibody-antigen interaction, we performed a negative control experiment, in which we compared the biosensor response toward SΔ19-VSV^{GFP}ΔG with its response to VSVΔG-G, a morphologically similar construct that lacks the spike protein. As seen in Fig. 4C, simply incubating either virus types on the biochip results in a similar impedance response (red bars). However, the detection specificity was revealed after briefly rinsing the biochip. As clearly shown in Fig. 4C (blue bars), rinsing did not have any effect on the ΔR_{ct} of SΔ19-VSV^{GFP}ΔG pseudovirus samples, whereas for the VSVΔG-G control samples, ΔR_{ct} recovered almost completely to its initial value (prior to incubation with virus). These results indicate that specific binding of spike-presenting pseudovirus can withstand rinsing, while a facile removal of a similar virion that lacks the antigen improves the signal-to-noise ratio. These results also imply that the immobilized S1Ab layer is sufficiently stable and yields reproducible response after removal of physically or loosely bound layers. To further test the selectivity of the biosensor and ensure that signals are specific we have added a mixture of nonspecific proteins to the measurement buffer and measured the impedance spectra for bare electrodes, S1Ab-functionalized and in the presence of RBD or SΔ19-VSV^{GFP}ΔG, as described in Supplementary section S5. The relative R_{ct} response was found to be similar to that obtained by the standard measurement buffer, as seen in Supplementary Fig. S6.

Further evidence for the biosensors' performance in detecting SARS-CoV-2 pseudovirus was obtained by measuring different SΔ19-VSV^{GFP}ΔG concentrations. As shown in Fig. 4D, a gradual increase in ΔR_{ct} was observed in response to increasing pseudovirus concentrations. A concentration of 10^4 pseudovirus particles/mL was sufficient to affect an average R_{ct} increase of 11% (±5). The recorded ΔR_{ct} values, also listed in Supplementary Table 3, exhibited an exponential dependence on pseudovirus concentration, similar to that previously observed for the purified antigen.

4. Discussion

Rapid POC diagnostic tools that can provide sensitive and quantitative detection of SARS-CoV-2 are needed to monitor the spread of COVID-19 within the community in real-time, accelerate accurate data acquisition, and make informed decisions concerning disease containment and "exit strategies". We have developed an impedimetric immunosensor, comprised of a miniaturized biochip, assembled into a portable measurement platform that enables simultaneous measurement of multiple biochips, provides electrical contacts, and interfaces with a potentiostat device. By optimizing microelectronic fabrication technology, chips were manufactured at a high yield and reproducibility, as verified by scanning electron microscopy and electrochemical characterization methods. Chips were biofunctionalized with thiol-modified anti-S1 mAbs. The employed direct functionalization strategy proved to be robust, yielding a stable antibody layer. The uniformity and stability of the immobilized mAb layer was previously investigated and reported by us [41]. This approach is advantageous compared to well-established self-assembled monolayer (SAM) generation methods since it involves a straightforward preparation and avoids complete electrode passivation often attained with SAM. To demonstrate the diagnostic potential of the developed biochip, we have applied label-free EIS measurement to detect low concentrations of SARS-CoV-2 spike protein RBD. The biosensor exhibited a detection range of concentrations spanning five orders of magnitude, which is a broader range compared to previously reported ELISA tests [42]. A concentration-dependent R_{ct} response was reproducible and a specific signal was obtained at an antigen concentration of 15 ng/mL (500 pM). A comparable detection limit was recently reported by time-resolved fluorescent ELISA tests, albeit with a much lower signal-to-noise ratio and a semi-quantitative readout [43]. The applicability of the immunosensor was further demonstrated by detecting virus particles. Our recently developed spike protein-pseudo-typed VSV platform was utilized as a model for SARS-CoV-2, which obviates the need for special biosafety requirements and brings many advantages such as morphological similarity, scalability, genetic stability, and compatibility with various orthogonal studies. A detection range of 10^4 to 10^9 pseudovirus particles/mL was demonstrated, which is superior to most commercially available Ag-RDT, as recently quantified by a manufacturer-independent evaluation of 19 marketed Ag-RDT [44]. Out

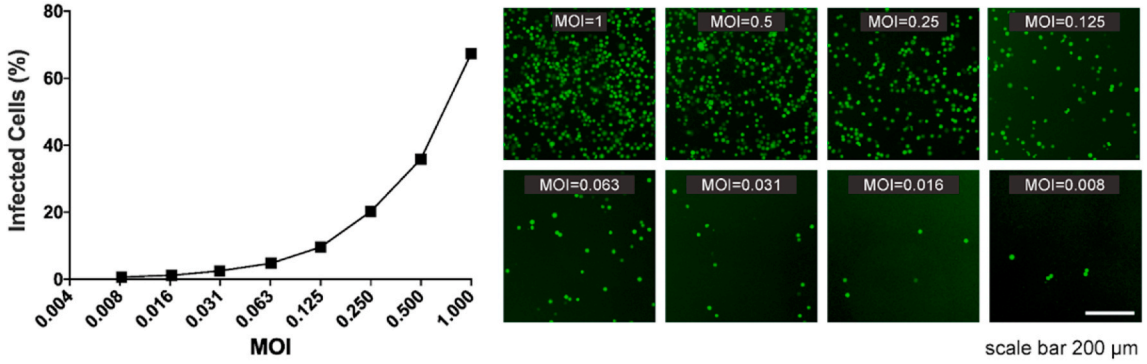

Fig. 3. Evaluation of SΔ19-VSV^{GFP}ΔG pseudovirus infection. Serial dilutions of SΔ19-VSV^{GFP}ΔG pseudoviruses were added at various MOIs to ACE2-expressing HEK293 cells for 24 h. Number of infected cells were counted using IncuCyte zoom software. Percentage of infected cells (shown left) was determined by quantifying the number of GFP-positive cells compared to the number of DAPI-stained nuclei.

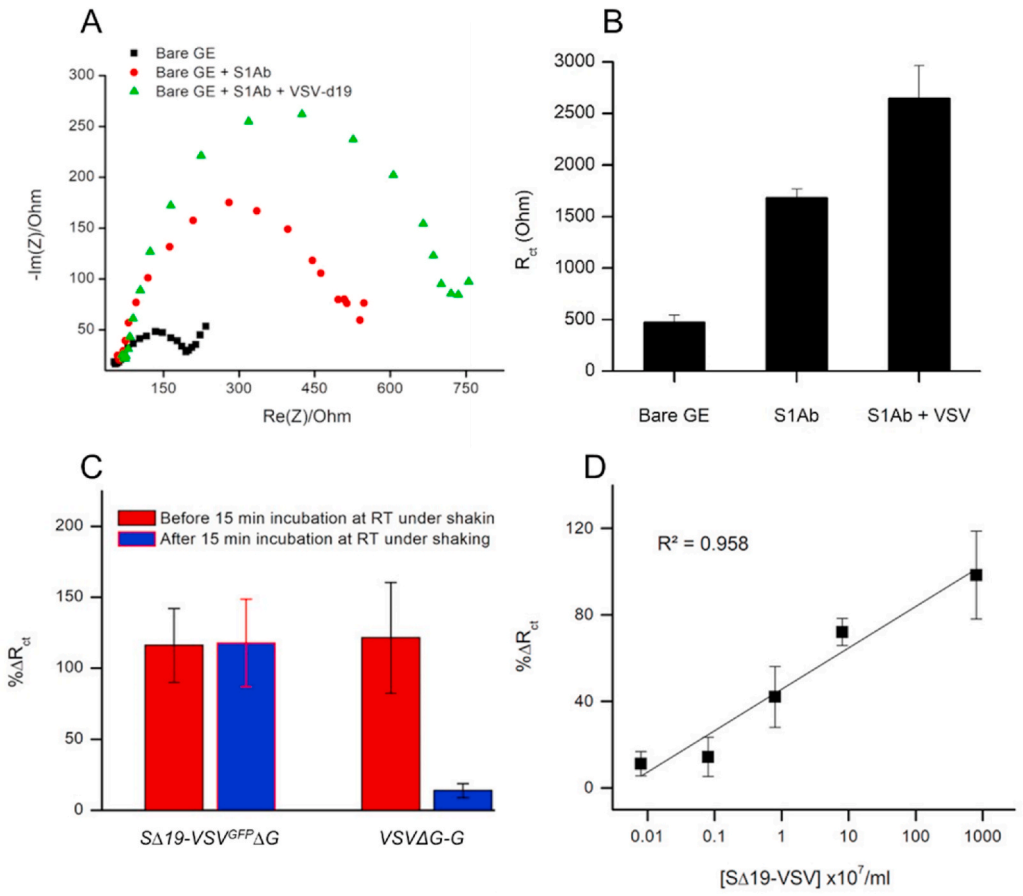

Fig. 4. Detection of SARS-CoV-2 pseudovirus. A) Representative Nyquist plots from measurements of a bare gold electrode (black squares), electrode after functionalization with S1Ab (red circles), and S1Ab-functionalized electrode after incubation in solution containing 2×10^7/mL SΔ19-VSV^{GFP}ΔG pseudovirus particles (green triangles). B. Corresponding R_{ct} values averaged over 3–5 repetitions. C. Comparison of $\%\Delta R_{ct}$ using SΔ19-VSV^{GFP}ΔG vs. VSVΔG-G. Red bars present $\%\Delta R_{ct}$ immediately after incubation with either SΔ19-VSV^{GFP}ΔG or VSVΔG-G and blue bars show the same electrodes after 15 min of subtle shaking at room temperature; D) Dependence of $\%\Delta R_{ct}$ on SΔ19-VSV^{GFP}ΔG concentration. Data represent the average of three independent experiments (6–8 repetitions each). Error bars represent ±SD. (For interpretation of the references to color in this figure legend, the reader is referred to the Web version of this article.)

of the 19, four exhibited the lowest LOD of $1.1{\cdot}10^5$ gcn/mL (gene copy number per milliliter) using, however, direct viral culture supernatant, which poses additional challenges. It should be noted, that estimated viral loads vary considerably between individuals, ranging from 10^6-10^{11} virus particles/mL for infected patients [45,46]. Again, a positive correlation between SΔ19-VSV^{GFP}ΔG concentrations to R_{ct} response was consistently recorded, exhibiting an exponential dependence ($R^2 = 0.96$). Nonlinear calibration curves have been previously reported in impedimetric biosensors [47,48]. It should be noted that despite the large variability observed at high target concentrations in both RBD and pseudovirus measurements (due to non-specific adsorption ([49]), the difference in the means of ΔR_{ct} measured for the highest virus concentration ($8{\cdot}10^9$ particles/mL) and the medium concentration ($8{\cdot}10^7$ particles/mL) was found to be statistically significant ($p\text{-value} < 0.0001$). Similarly, in the RBD measurements, the difference between the mean ΔR_{ct} of the highest concentration (1550 μg/mL) and the medium concentration (155 μg/mL) was also found to be statistically significant ($p = 0.01$). More importantly, nonspecific binding of VSVΔG-G that lacks the spike protein was not observed, demonstrating the specificity of the immunosensors. Furthermore, addition of non-specific proteins to the measurement buffer did not have any observable effect on the recorded signal lending further support to the selectivity of the biosensor and the feasibility of the detection method.

It is interesting to compare the effect on R_{ct} elicited by whole pseudovirus particles and solubilized spike antigens (S1-RBD). In theory, a larger effect on R_{ct} is expected by binding of the whole virus particle. This is evident in the $\%\Delta R_{ct}$ affected by the lowest antigen concentrations. While binding of $3{\cdot}10^{-10}$ M S1-RBD was shown to increase the average R_{ct} by 33%(±7), an increase of $R_{ct} = 11\%(\pm 5)$ resulted from the binding of $\sim 10^4$ virus particles/mL that reportedly express much lower antigen concentrations [50,51]. Further study is needed to correlate the soluble antigens' binding capacity and resulted signal with that of a whole virus particle.

We have shown that despite obvious limitations related to nonspecific adsorption and sample inhomogeneity, the developed biosensor provides a concentration-dependent signal that can be fit to an exponential function yielding a calibration curve. Overall, the developed biosensor improves on other Ag-RDT, including recently reported electrochemical immunosesning platforms.

5. Conclusions

Electrochemical and electronic-based miniaturized diagnostic devices emerge as a promising alternative to traditional diagnostic techniques. We have developed an immunosensor that is leveraging the advantages of microelectronic fabrication and may significantly expand our diagnostic capacity. Most importantly, it greatly simplifies sample preparation, capable of selectively detecting low viral loads and allows for a straightforward measurement of various sample types. Future applications may be aimed at monitoring and understanding viral load dynamics, which is a fundamental aspect of the COVID-19 pandemic. Although intensively studied, the correlation between viral load and infectiousness is still unclear. A rapid POC device that has the potential to determine viral loads may provide clinical and epidemiological important information.

Author contribution

S.F, I.A and M.G.T conceptualized the idea, I.A designed and performed the experiments and analyzed the data, S.F and I.A wrote the manuscript, M.G.T, M.D, M.W and J.A, developed the pseudivirus, A.O fabricated the biochips.

Credit author statement

Idan Ashur: Conceptualization, Methodology, Investigation, Formal analysis, Validation; Michal Werbner: Methodology, Investigation, Validation; Joel Alter: Methodology, Investigation, Validation; Abraham Ogungbile: Methodology, Validation, Resources; Moshe Dessau: Methodology, Validation, Resources, Visualization; Meital Gal-Tanamy: Methodology, Validation, Resources, Visualization, Funding acquisition; Sefi Vernick: Conceptualization, Methodology, Resources, Writing – Original Draft, Writing-Review & Editing, Visualization, Supervision, Project administration, Funding acquisition.

Funding information

The research was supported by the Israel Innovation Authority and Mekorot Israel National Water company (Grant Number: 71037, to S.V); The Ministry of Science, And Technology (grant number 16909–3, to M. G.T.); The Dangoor Center for Personalized Medicine, Bar-Ilan University (to M. G.T. and M. D.), and by Israel Science Foundation (grant number 3711/20, to M. G.T).

Declaration of competing interest

The authors declare that they have no known competing financial interests or personal relationships that could have appeared to influence the work reported in this paper.

Acknowledgments

We wish to thank Mr Itzik Icin from the Bioelectronics lab, Volcani center for his kind assistance with fabrication processes. We also greatly appreciate the assitance of Roy Posmanic, Matat Zohar, and Ezra Orlofski from Newe Ya'ar Research Center, Agricultural Research Organization – Volcani Institute, in providing the organic-supplemented solutions.

Appendix A. Supplementary data

Supplementary data to this article can be found online at https://doi.org/10.1016/j.talanta.2021.123147.

References

[1] FIND, (Foundation for innovative new diagnostics) TEST DIRECTORY. 4 may 2021. https://www.finddx.org/test-directory/, 2021.
[2] Peeling, R.W., Olliaro, P.L., Boeras, D.I., Fongwen, N., Scaling up COVID-19 rapid antigen tests: promises and challenges. The Lancet Infectious Diseases.
[3] A. Berger, M.T.N. Nsoga, F.J. Perez-Rodriguez, Y.A. Aad, P. Sattonnet-Roche, A. Gayet-Ageron, I. Eckerle, Diagnostic accuracy of two commercial SARS-CoV-2 antigen-detecting rapid tests at the point of care in community-based testing centers, PLoS One 16 (3) (2021), e0248921.
[4] CDC, Overview of Testing for SARS-CoV-2 (COVID-19), 2021.
[5] D.B. Larremore, B. Wilder, E. Lester, S. Shehata, J.M. Burke, J.A. Hay, R. Parker, Test sensitivity is secondary to frequency and turnaround time for COVID-19 screening, Science Advances 7 (1) (2021), eabd5393.
[6] S. Ricks, E.A. Kendall, D.W. Dowdy, J.A. Sacks, S.G. Schumacher, N. Arinaminpathy, Quantifying the potential value of antigen-detection rapid diagnostic tests for COVID-19: a modelling analysis, BMC Med. 19 (1) (2021) 75.
[7] CDC, Interim Laboratory Biosafety Guidelines for Handling and Processing Specimens Associated with Coronavirus Disease 2019 (COVID-19), 2021.
[8] D.S. Khoury, A.K. Wheatley, M.D. Ramuta, A. Reynaldi, D. Cromer, K. Subbarao, M. P. Davenport, Measuring immunity to SARS-CoV-2 infection: comparing assays and animal models, Nat. Rev. Immunol. 20 (12) (2020) 727–738.
[9] F. Schmidt, Y. Weisblum, F. Muecksch, H.H. Hoffmann, E. Michailidis, J.C. C. Lorenzi, P.D. Bieniasz, Measuring SARS-CoV-2 neutralizing antibody activity using pseudotyped and chimeric viruses, J. Exp. Med. 217 (11) (2020).
[10] W. Wang, E.N. Butler, V. Veguilla, R. Vassell, J.T. Thomas, M. Moos, C.D. Weiss, Establishment of retroviral pseudotypes with influenza hemagglutinins from H1, H3, and H5 subtypes for sensitive and specific detection of neutralizing antibodies, J. Virol Methods 153 (2) (2008) 111–119.
[11] S.N. Neerukonda, R. Vassell, R. Herrup, S. Liu, T. Wang, K. Takeda, C.D. Weiss, Establishment of a well-characterized SARS-CoV-2 lentiviral pseudovirus neutralization assay using 293T cells with stable expression of ACE2 and TMPRSS2, PLoS One 16 (3) (2021), e0248348.
[12] I. Zucker, Y. Lester, J. Alter, M. Werbner, Y. Yecheskel, M. Gal-Tanamy, M. Dessau, Pseudoviruses for the assessment of coronavirus disinfection by ozone, Environ. Chem. Lett. 19 (2) (2021) 1779–1785.
[13] D. Pinto, Y.-J. Park, M. Beltramello, A.C. Walls, M.A. Tortorici, S. Bianchi, D. Corti, Cross-neutralization of SARS-CoV-2 by a human monoclonal SARS-CoV antibody, Nature 583 (7815) (2020) 290–295.
[14] M. Letko, A. Marzi, V. Munster, Functional assessment of cell entry and receptor usage for SARS-CoV-2 and other lineage B betacoronaviruses, Nature Microbiology 5 (4) (2020) 562–569.
[15] J. Nie, Q. Li, J. Wu, C. Zhao, H. Hao, H. Liu, Y. Wang, Establishment and validation of a pseudovirus neutralization assay for SARS-CoV-2, Emerg. Microb. Infect. 9 (1) (2020) 680–686.
[16] H.L. Xiong, Y.T. Wu, J.L. Cao, R. Yang, Y.X. Liu, J. Ma, N.S. Xia, Robust neutralization assay based on SARS-CoV-2 S-protein-bearing vesicular stomatitis virus (VSV) pseudovirus and ACE2-overexpressing BHK21 cells, Emerg. Microb. Infect. 9 (1) (2020) 2105–2113.
[17] F. Zettl, T.L. Meister, T. Vollmer, B. Fischer, J. Steinmann, A. Krawczyk, G. Zimmer, Rapid quantification of SARS-CoV-2-neutralizing antibodies using propagation-defective vesicular stomatitis virus pseudotypes, Vaccines 8 (3) (2020).
[18] M. Chen, X.-E. Zhang, Construction and applications of SARS-CoV-2 pseudoviruses: a mini review, Int. J. Biol. Sci. 17 (6) (2021) 1574–1580.
[19] J. Nie, Q. Li, J. Wu, C. Zhao, H. Hao, H. Liu, Y. Wang, Quantification of SARS-CoV-2 neutralizing antibody by a pseudotyped virus-based assay, Nat. Protoc. 15 (11) (2020) 3699–3715.
[20] J.M. Condor Capcha, G. Lambert, D.M. Dykxhoorn, A.G. Salerno, J.M. Hare, M. A. Whitt, L.A. Shehadeh, Generation of SARS-CoV-2 spike pseudotyped virus for viral entry and neutralization assays: a 1-week protocol, Frontiers in Cardiovascular Medicine 7 (381) (2021).
[21] Y. Yan, L. Chang, W. Luo, J. Liu, F. Guo, L. Wang, Comparison of seven commercial severe acute respiratory syndrome coronavirus 2 nucleic acid detection reagents with pseudovirus as quality control material, J. Mol. Diagn. 23 (3) (2021) 300–309.
[22] K.M. Koczula, A. Gallotta, Lateral flow assays, Essays Biochem. 60 (1) (2016) 111–120.
[23] M. Pohanka, Point-of-Care diagnoses and assays based on lateral flow test, International Journal of Analytical Chemistry 2021 (2021) 6685619.
[24] A.J. Bard, L.R. Faulkner, Electrochemical Methods : Fundamentals and Applications, second ed., Wiley, New York, 2001.
[25] E.P. Randviir, C.E. Banks, Electrochemical impedance spectroscopy: an overview of bioanalytical applications, Analytical Methods 5 (5) (2013) 1098–1115.
[26] M.O. Shaikh, B. Srikanth, P.-Y. Zhu, C.-H. Chuang, Impedimetric immunosensor utilizing polyaniline/gold nanocomposite-modified screen-printed electrodes for early detection of chronic kidney disease, Sensors 19 (18) (2019) 3990.
[27] Y.-H. Yun, A. Bhattacharya, N.B. Watts, M.J. Schulz, A label-free electronic biosensor for detection of bone turnover markers, Sensors 9 (10) (2009) 7957–7969.
[28] A. Ahmed, J.V. Rushworth, J.D. Wright, P.A. Millner, Novel impedimetric immunosensor for detection of pathogenic bacteria Streptococcus pyogenes in human saliva, Anal. Chem. 85 (24) (2013) 12118–12125.
[29] S. Siddiqui, Z. Dai, C.J. Stavis, H. Zeng, N. Moldovan, R.J. Hamers, P. U. Arumugam, A quantitative study of detection mechanism of a label-free impedance biosensor using ultrananocrystalline diamond microelectrode array, Biosens. Bioelectron 35 (1) (2012) 284–290.
[30] Y. Saylan, O. Erdem, S. Unal, A. Denizli, An alternative medical diagnosis method: biosensors for virus detection, Biosensors 9 (2) (2019).
[31] D. Nidzworski, K. Siuzdak, P. Niedzialkowski, R. Bogdanowicz, M. Sobaszek, J. Ryl, T. Ossowski, A rapid-response ultrasensitive biosensor for influenza virus detection using antibody modified boron-doped diamond, Sci. Rep. 7 (1) (2017) 15707.
[32] A.D. Chowdhury, K. Takemura, T.-C. Li, T. Suzuki, E.Y. Park, Electrical pulse-induced electrochemical biosensor for hepatitis E virus detection, Nat. Commun. 10 (1) (2019) 3737.
[33] A. Kaushik, A. Yndart, S. Kumar, R.D. Jayant, A. Vashist, A.N. Brown, M. Nair, A sensitive electrochemical immunosensor for label-free detection of Zika-virus protein, Sci. Rep. 8 (1) (2018) 9700.
[34] J.H. Kim, C.H. Cho, M.Y. Ryu, J.G. Kim, S.J. Lee, T.J. Park, J.P. Park, Development of peptide biosensor for the detection of dengue fever biomarker, nonstructural 1, PLoS One 14 (9) (2019), e0222144.
[35] L.A. Layqah, S. Eissa, An electrochemical immunosensor for the corona virus associated with the Middle East respiratory syndrome using an array of gold nanoparticle-modified carbon electrodes, Mikrochim. Acta 186 (4) (2019) 224.
[36] B. Mojsoska, S. Larsen, D.A. Olsen, J.S. Madsen, I. Brandslund, F.A. Alatraktchi, Rapid SARS-CoV-2 detection using electrochemical immunosensor, Sensors 21 (2) (2021).
[37] Y. Hillman, J. Gershberg, D. Lustiger, D. Even, D. Braverman, Y. Dror, Y. Wine, Monoclonal antibody-based biosensor for point-of-care detection of type III secretion system expressing pathogens, Anal. Chem. 93 (2) (2021) 928–935.
[38] N.G. Welch, J.A. Scoble, B.W. Muir, P.J. Pigram, Orientation and characterization of immobilized antibodies for improved immunoassays, Biointerphases 12 (2) (2017).
[39] M.P. Chatrathi, J. Wang, G.E. Collins, Sandwich electrochemical immunoassay for the detection of Staphylococcal enterotoxin B based on immobilized thiolated antibodies, Biosens. Bioelectron. 22 (12) (2007) 2932–2938.

[40] A. Lasia, Impedance of the faradaic reactions in the presence of mass transfer. Electrochemical Impedance Spectroscopy and its Applications, Springer New York, New York, NY, 2014, pp. 85–125.
[41] A.O. Ogungbile, I. Ashur, I. Icin, O.H. Shapiro, S. Vernick, Rapid detection and quantification of microcystins in surface water by an impedimetric immunosensor, Sensor. Actuator. B Chem. 348 (2021) 130687.
[42] J.-H. Lee, M. Choi, Y. Jung, S.K. Lee, C.-S. Lee, J. Kim, H.G. Kim, A novel rapid detection for SARS-CoV-2 spike 1 antigens using human angiotensin converting enzyme 2 (ACE2), Biosens. Bioelectron. 171 (2021), 112715-112715.
[43] M. Barlev-Gross, S. Weiss, A. Ben-Shmuel, A. Sittner, K. Eden, N. Mazuz, A. Mechaly, Spike vs nucleocapsid SARS-CoV-2 antigen detection: application in nasopharyngeal swab specimens, Anal. Bioanal. Chem. 413 (13) (2021) 3501–3510.
[44] A.I. Cubas-Atienzar, K. Kontogianni, T. Edwards, D. Wooding, K. Buist, C. R. Thompson, E.R. Adams, Limit of detection in different matrices of nineteen commercially available rapid antigen tests for the detection of SARS-CoV-2, medRxiv 2021 (2003) (2021) 21253950, 2019.
[45] H. Kawasuji, Y. Takegoshi, M. Kaneda, A. Ueno, Y. Miyajima, K. Kawago, Y. Yamamoto, Transmissibility of COVID-19 depends on the viral load around onset in adult and symptomatic patients, PLoS One 15 (12) (2020), e0243597.
[46] K.A. Walsh, K. Jordan, B. Clyne, D. Rohde, L. Drummond, P. Byrne, P. Harrington, SARS-CoV-2 detection, viral load and infectivity over the course of an infection, J. Infect. 81 (3) (2020) 357–371.
[47] M. Barreiros dos Santos, C. Sporer, N. Sanvicens, N. Pascual, A. Errachid, E. Martinez, J. Samiter, Detection of pathogenic bacteria by electrochemical impedance spectroscopy: influence of the immobilization strategies on the sensor performance, Procedia Chemistry 1 (1) (2009) 1291–1294.
[48] L. Lu, G. Chee, K. Yamada, S. Jun, Electrochemical impedance spectroscopic technique with a functionalized microwire sensor for rapid detection of foodborne pathogens, Biosens. Bioelectron. 42 (2013) 492–495.
[49] A. Ahluwalia, G. Giusto, D. DeRossi, Non-specific adsorption on antibody surfaces for immunosensing, Mat Sci Eng C-Bio S 3 (3–4) (1995) 267–271.
[50] Z. Ke, J. Oton, K. Qu, M. Cortese, V. Zila, L. McKeane, J.A.G. Briggs, Structures and distributions of SARS-CoV-2 spike proteins on intact virions, Nature 588 (7838) (2020) 498–502.
[51] H.P. Yao, Y.T. Song, Y. Chen, N.P. Wu, J.L. Xu, C.J. Sun, S. Li, Molecular architecture of the SARS-CoV-2 virus, Cell 183 (3) (2020) 730–+.